

Turbulent fluctuations and the excitation of Z Cam outbursts

Johnathan Ross^{1*}, Henrik N. Latter¹

¹ DAMTP, University of Cambridge, CMS, Wilberforce Road Cambridge CB3 0WA, UK

ABSTRACT

Z Cam variables are a subclass of dwarf nova that lie near a global bifurcation between outbursting (‘limit cycle’) and non-outbursting (‘standstill’) states. It is believed that variations in the secondary star’s mass-injection rate instigate transitions between the two regimes. In this paper we explore an alternative trigger for these transitions: stochastic fluctuations in the disk’s turbulent viscosity. We employ simple one-zone and global viscous models which, though inappropriate for detailed matching to observed light curves, clearly indicate that turbulent disk fluctuations induce outbursts when the system is sufficiently close to the global bifurcation point. While the models easily produce the observed ‘outburst/dip’ pairs exhibited by Z Cam and Nova-like variables, they struggle to generate long trains of outbursts. We conclude that mass transfer variability is the dominant physical process determining the overall Z Cam standstill/outburst pattern, but that viscous stochasticity provides an additional ingredient explaining some of the secondary features observed.

Key words: accretion, accretion disks — stars: dwarf nova — nova, cataclysmic variables — turbulence

1 INTRODUCTION

Dwarf novae (DNe), a subclass of cataclysmic variables, are binary systems where matter overflows the Roche-lobe of a main sequence star and forms a disk around a white dwarf primary. Typically, observations show large, regular variation in luminosity with timescales between a few days and a few years, and with a magnitude jump of between 2 and 6. It is believed that this variation issues from a thermal instability in the accretion disk owing to profound changes in the disk’s opacity near the ionisation temperature of hydrogen (Hōshi 1979, Meyer & Meyer-Hofmeister 1981, Faulkner et al 1983, hereafter FLP).

One of the more intriguing subclasses of DNe are the Z Cam variables, whose decay from outburst may be interrupted by long *standstills*. These correspond to periods where the luminosity remains roughly constant for months to years (Warner 1995). Standstills are followed by a rapid drop to quiescence and the initiation of a fresh train of outbursts (Simonsen et al, 2014). In some systems, standstills are punctuated by isolated ‘outburst/dip’ pairs, for example in the prototype itself, Z Camelopardalis. An example pair is plotted in Figure 1. The nova-like class of cataclysmic variables also show occasional (though stunted) outbursts, such as UU Aqr, Q Cyg, and CP Lac (Honeycutt et al 1998, Hon-

eycutt 2001). Note that within the Z Cam group, there are outliers with even more exotic behaviour. For example, the lightcurves of IW And and V513 Cas show rises to outburst *from* standstill (Simonsen et al. 2014).

It was understood early in the development of the disk instability model that this behaviour could be explained by variation in the mass transfer rate from the main sequence secondary star (Meyer & Meyer-Hofmeister 1983, Lin et al. 1985, Buat-Ménard et al. 2001, Lasota 2001). When the transfer is too great then the system remains in the high state indefinitely; but if below a critical value the system enters the recurrently outbursting state. Z Cam variables are believed to straddle the bifurcation point demarcating these two regimes, with variations in the transfer rate pushing the system into one or the other. The critical rate depends on parameters such as the binary mass ratio, disk viscosity, disk radius, etc., and variations in the injection rate may be caused by irradiation of the secondary (Smak, 1996), a solar type cycle (Livio & Pringle, 1994), or starspots (King and Cannizzo 1998).

Turbulent stresses in the disk facilitate accretion of the transferred material, while also providing the heating mechanism. But turbulence is fundamentally chaotic in nature, producing fluctuations on the orbital timescale and longer (e.g. Hawley et al. 1995), and these constitute an important feature of the flow. For example, the propagation of such viscous fluctuations can explain the log-normality

* E-mail: jpr2@cam.ac.uk

and rms-flux relation in X-ray binaries and AGN (Uttley & McHardy 2001, Ingram & van der Klis 2013, Cowperthwaite & Reynolds 2014). Another example concerns their effects on the thermal stability of X-ray binaries (Janiuk & Misra 2012) and on thermal instability in general (Ross et al 2017). In this paper we examine the role of turbulent fluctuations in triggering outbursts from standstill in DNe. For most mass transfer rates, fluctuations do not endanger the coherence of the limit cycle (see MRI simulations by Latter & Papaloizou 2012 and Hirose et al. 2014) and hence may be ‘smoothed out’ with an eddy-viscosity model. However, for systems perched on criticality, turbulent variations in the mass accretion rate may easily instigate limit cycles, and can no longer be neglected. Such noisy critical systems have multiple analogues, perhaps the closest being the Fitzhugh-Nagumo (FHN) model for signal transmission along nerves. Indeed, fluctuation-induced limit cycles have been observed and extensively studied in that context (Treutlein & Schulten 1985, 1986).

We employ two, relatively simple, models to explore this behaviour. The first is a one-zone representation of the surface density and central temperature in a disk annulus at an outer radius. Essentially, it combines the surface density evolution equation of Mineshige & Osaki (1983) and the reduced thermodynamical approach of FLP, while adding a stochastic alpha viscosity. The result is a noisy two-dimensional dynamical system, similar in most respects to the FHN equations. We also make use of a global one-dimensional viscous disk model, drawn from the work of Papaloizou et al. (1983), Lin et al. (1985) and Cannizzo (1993a), but which includes a stochastically varying viscosity. It thus has some features in common with the model of Janiuk & Misra (2012), which describes the radiation-pressure dominated flows around black holes.

Our results show that fluctuations alone can induce limit cycles from standstills leading to individual, or occasionally repeated, outbursts as observed in some Z Cam and nova-like cataclysmic variables. U Gem type behaviour is also produced for a mass transfer rate above the classical critical value if the turbulent amplitude is sufficiently large. However, long trains of outbursts separated by long standstills are not a natural outcome of the simulations, unless we also include mass transfer variation from the secondary. The results suggest that turbulent fluctuations are an important, previously omitted, ingredient in DN modelling, complementary to mass transfer variability but by no means a replacement.

The plan of the paper is as follows. In Section 2 we introduce the 1D viscous disk model for DNe. In Section 3 we reduce the problem to a one-zone model to illustrate the idea of stochastic excitability both with and without mass transfer variability. Section 4 then demonstrates that this local phenomenon translates to a quasi-global disk setting. We discuss our results in Section 5.

2 VISCOUS DISK MODEL

One of the simplest ways of modelling an accretion disk is to conduct a global vertical and azimuthal average. Then, with some additional weak assumptions, we obtain a single equation for surface density in radius and time. If the tur-

bulence in the disk is modelled by an eddy viscosity, the surface density

$$\Sigma(r) = \int_{-\infty}^{\infty} \rho dz, \quad (1)$$

obeys the nonlinear diffusion equation (Pringle 1981),

$$\frac{\partial \Sigma}{\partial t} = \frac{3}{r} \frac{\partial}{\partial r} \left[r^{1/2} \frac{\partial}{\partial r} (r^{1/2} \nu \Sigma) \right] + S(r, t), \quad (2)$$

where ν is the kinematic viscosity, in general a function of surface density, midplane temperature T_c , and radius. The term S represents the source of mass from the secondary. The disk is assumed to be Keplerian.

In order to describe the evolution of the midplane temperature, we call on the vertically integrated, thin-disk, energy equation

$$C_P \frac{DT_c}{Dt} = \frac{9\nu\Omega^2}{4} - \frac{2F_s}{\Sigma} - \frac{2H}{r\Sigma} \frac{\partial(rF_r)}{\partial r} - \frac{\mathcal{R}T_c}{\mu} \frac{1}{r} \frac{\partial(rv_r)}{\partial r}. \quad (3)$$

We have used the form of this equation favoured by Cannizzo (1993a, see also Lasota 2001). The material derivative, $D(\cdot)/Dt$, includes the contribution from radial advection, $v_r \partial(\cdot)/\partial r$, as well as the local change with time, $\partial(\cdot)/\partial t$. The radial advection speed is due to accretion and can be written in terms of the viscous stress. The disk semi-thickness is H , C_P is the specific heat, μ is molecular mass, and \mathcal{R} is the gas constant.

The first term on the right hand-side is the local vertically integrated viscous dissipation. This is followed by the local radiative cooling rate, where F_s is the flux emitted by each disk surface. The next describes radial radiative transport of energy, where F_r is the radiative flux in the radial direction, given by

$$F_r = - \frac{2H\sigma T_c^3}{\kappa\Sigma} \frac{\partial T_c}{\partial r}, \quad (4)$$

where κ is the opacity. The last term on the right hand side represents the energy released by PdV work where \mathcal{R} is the ideal gas constant.

In order to calculate the radiative cooling at the surfaces, the disk’s vertical structure must be determined at each radius (Lasota, 2001), necessitating the inclusion of radiative transport, the gas’s ionisation state, etc. Our aim, however, is to sketch out the qualitative behaviour of the dynamics rather than match observations in detail, and so we adopt the simpler, somewhat more transparent approach, of FLP who model the dependence of cooling rate on T_c via a set of analytical, physically motivated prescriptions which we now summarise.

It is assumed that the disk is emitting as a black body and so F_s is given by

$$F_s = \sigma T_e^4, \quad (5)$$

where σ is the Stefan-Boltzmann constant and T_e is the effective temperature, related to T_c by taking into account the vertical structure of the disk. The connection between T_e and T_c may be determined by considering three temperature regimes, distinguished by the ionization fraction of hydrogen. For each regime a different parametrisation for T_e is necessary.

(i) The first is when the disk is mostly ionised and is in the hot optically thick state, with $T_c > 10^4$ K. In this case

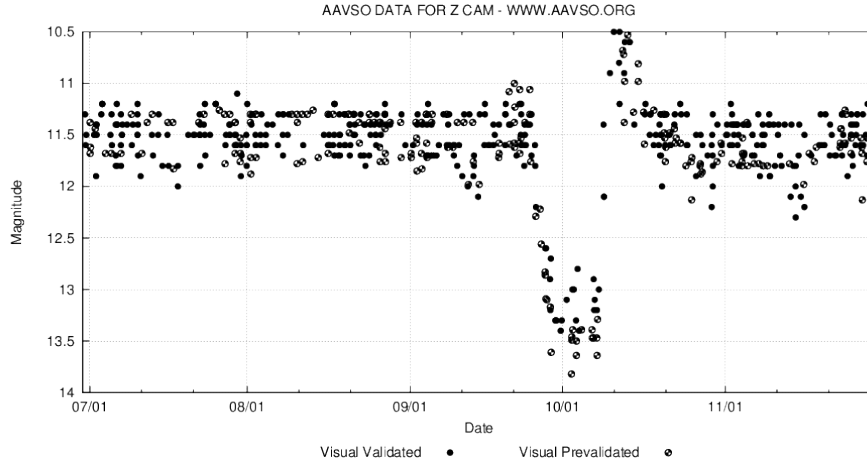


Figure 1. Isolated outburst/dip in the lightcurve of Z Cam during a standstill (1981 July to 1981 December). Data from the AAVSO.

the majority of the optical depth originates from near the mid-plane. This leads to the relation

$$T_{e1}^4 = \frac{4}{3} \frac{T_c^4}{\tau_c}, \quad (6)$$

where τ_c is the mid-plane optical depth given by $\tau_c = \kappa_{c1} \Sigma$. The opacity in regime 1 may be approximated by Kramer's formula,

$$\kappa_{c1} = 1.5 \times 10^{20} \frac{\Sigma}{2H} T^{-2.5}. \quad (7)$$

(ii) The next regime is when hydrogen is partially ionized in the mid-plane but the cold photosphere is mostly neutral. There is a sharp drop-off in ionisation with height when the temperature drops through the ionisation threshold. An abrupt change in opacity results and the dependence of effective temperature T_{e2} on central temperature T_c becomes very weak. In fact, we have

$$T_{e2} = \left(10^{36} E \left(\frac{\Sigma}{2H} \right)^{-1/3} / \Sigma \right)^{1/10}, \quad (8)$$

where E is dimensionless constant that can be optimised to improve the approximation.

(iii) The last regime is when the whole vertical extent of the disk is cold and poorly ionised, $T_c < 4000$ K. Then we may approximate the relationship between effective and central temperatures by

$$T_{e3} = (2\lambda\tau_c)^{1/4} T_c, \quad (9)$$

where λ is another dimensionless constant. As in regime (ii), the opacity is dominated by H^- ions and may be approximated by

$$\kappa_{c3} = 10^{-36} \left(\frac{\Sigma}{2H} \right)^{1/3} T^{10}. \quad (10)$$

In the above 3 expressions for T_{ci} , the quantities are in CGS units. To prevent discontinuities when matching these three expressions, we adopt

$$T_e^4 = \frac{(T_{e1}^4 + T_{e2}^4) T_{e3}^4}{\left(\sqrt{(T_{e1}^4 + T_{e2}^4)} + T_{e3}^2 \right)^2}. \quad (11)$$

For a more detailed discussion of the radiative cooling model we refer the reader to FLP and Latter & Papaloizou (2012). We choose $E = 5.66$ and $\lambda = 0.5$, as in FLP.

Note that the FLP model is a crude simplification of the full vertical radiative transfer problem, and performs poorly on the lower stable branch of solutions. However, on the hot upper branch, in which we are primarily interested in this paper, it is more reliable. Some of the model's peculiarities include (a) an exaggerated 'elongation' of the S-curve in the Σ axis: the two corners of the 'S' differ by a factor of 3 or more, in contrast to more realistic curves obtained from vertical integrations (e.g. Meyer & Meyer-Hofmeister 1981); (b) the scalings of these corners with disk parameters, such as α , also differ from the vertical integrations (e.g. Hameury et al. 1998); (c) detailed features of obtained light curves are not reproduced correctly. See Cannizzo (1993b) for criticisms of the model. That all being said, for our purposes (proof of concept) the FLP approach is more than adequate, and furthermore very convenient.

To close the system of equations, we adopt the α -model to express ν in terms of the other variables, and so explicitly link the two evolution equations (Shakura & Sunyaev, 1973). We stipulate that

$$\nu = \frac{2}{3} \alpha \frac{\mathcal{R} T_c}{\mu \Omega}. \quad (12)$$

In this work α is a stochastic function of time through which we incorporate the effects of fluctuations in stress. The details of how this is modelled are given in the following sections.

In summary, the partial differential equations (2)-(3), along with the supplementary equations (4) - (12) and appropriate boundary conditions, approximate the time evolution of a 1D dwarf nova disk.

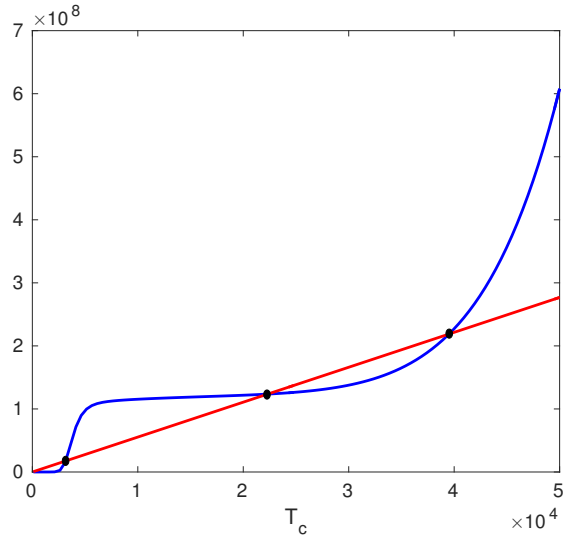


Figure 2. Cooling, Λ (blue) and heating, \mathcal{H} , (red) as functions of T_c for $\Sigma = 300 \text{ g cm}^{-2}$ and $\Omega = 2.22 \times 10^{-3} \text{ s}^{-1}$. The black dots correspond to the 3 thermal equilibria.

3 LOCAL ONE ZONE MODEL

3.1 Reduced dynamical system

3.1.1 Evolutionary equations

To fix ideas we begin our discussion with a reduced system. Consider an annulus at fixed radius $r = R$ and radial extent ΔR . Next assume that mass is injected into the annulus at rate \dot{M} and that its neighbouring annuli are in steady state. Mineshige and Osaki (1983) derive a convenient first order ODE for the surface mass density of such an annulus

$$\frac{d\Sigma}{dt} = -2 \left(\frac{R}{\Delta R} \right)^2 \frac{W - W_0}{(GM R)^{1/2}}, \quad (13)$$

where M is the mass of the central star and $W = 2\alpha PH$ is the vertically integrated viscous stress. We denote by W_0 its value in steady state,

$$W_0 = \frac{(GM)^{1/2}}{2\pi R^{3/2}} \left[1 - \left(\frac{R_*}{R} \right)^{1/2} \right] \dot{M}, \quad (14)$$

which is the stress the disk requires in order to process the injected mass from the secondary without any local build up (or evacuation) of mass. (Here R_* is the radius of the white dwarf.) If the actual stress in the annulus W is below or greater than W_0 then the mass of the annulus changes.

Using the α -prescription, Equation (13) can be rewritten as the nonlinear ODE

$$\frac{d\Sigma}{dt} = a_1 - a_2 \alpha \Sigma T_c, \quad (15)$$

where the constants a_1 and a_2 are given by

$$a_1 = \frac{\dot{M}}{\pi(\Delta R)^2} \left[1 - \left(\frac{R_*}{R} \right)^{1/2} \right], \quad a_2 = \frac{\mathcal{R}}{\mu \Omega (\Delta R)^2}, \quad (16)$$

and α may depend on time.

Turning now to the energy equation, we neglect advection, heating through compression, and radial radiative transport. The change in temperature of the annulus is determined solely from the competition between the viscous

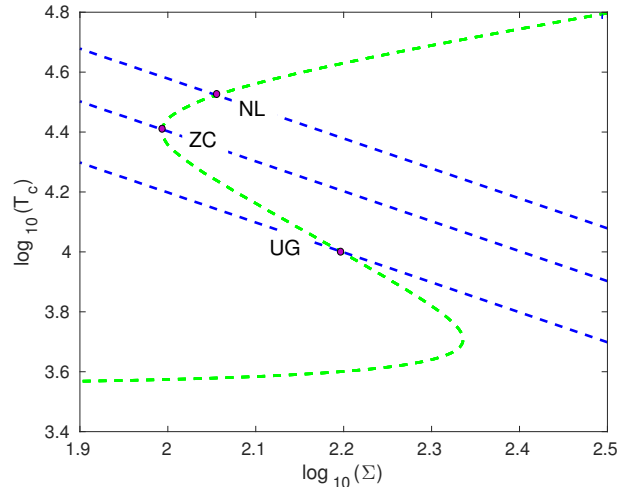


Figure 3. A single T -nullcline (green) and three Σ -nullclines (blue) corresponding to three different mass injection rates. Intersections of the curves correspond to fixed points of the system. Fixed points on the upper branch are stable, and the disk is always in the hot, highly accreting state. Such systems may correspond to Nova-like variables (NL). Fixed points on the middle branch are unstable and the system undergoes limit cycles. Such systems correspond to U Gem variables (UG). If the intersection point is just above the left corner of the T -nullcline (the saddle node), then perturbations to the accretion rate can easily move the Σ nullclines to the unstable middle branch precipitating a train of outbursts. Such systems are identified with the Z Cam class of variables (ZC). The three mass injection rates are 6, 4, and $2.5 \times 10^{16} \text{ g s}^{-1}$ respectively.

heating, \mathcal{H} , and radiative cooling, Λ , defined below. The thermal energy equation (3) is then

$$C_P \frac{dT_c}{dt} = a_3 \alpha T_c - \frac{2}{\Sigma} F_s(T_c, \Sigma), \quad (17)$$

$$= \mathcal{H} - \Lambda, \quad (18)$$

where the constant a_3 is

$$a_3 = \frac{3 \Omega \mathcal{R}}{2 \mu}. \quad (19)$$

The surface flux of energy F_s is computed from Eqs (5)-(11).

The viscous variation of Σ occurs on a timescale of

$$t_\Sigma = \frac{(\Delta R)^2}{\alpha H^2 \Omega}, \quad (20)$$

while the thermal timescale is roughly $t_{\text{th}} \sim 1/(\alpha \Omega)$, and is hence $\varepsilon^2 = H^2/(\Delta R)^2 \ll 1$ shorter. The dynamical system then exhibits ‘fast-slow’ dynamics and may be described by dimensionless equations

$$\frac{d\Sigma}{dt} = f(\Sigma, T_c, t), \quad \frac{dT_c}{dt} = \frac{1}{\varepsilon^2} g(\Sigma, T_c, t),$$

for nonlinear functions f and g , derived from Eqs (15) and (17). The second (thermal) equation varies much faster than the first (density) equation. While the surface density evolves on t_Σ , the system remains near to thermal equilibrium, hugging the curve given by $g \approx 0$ in the phase space of (Σ, T_c) . Only when thermal equilibrium is lost does the second equation ‘activate’ and there is rapid variation on t_{th} : an outburst or drop to quiescence.

3.1.2 Nullclines

In Figure 2 we plot examples of heating and cooling curves for an annulus in the outer disk at fixed Σ and constant α . The non-zero intersections give the thermal equilibria, $dT_c/dt = 0$, of which there can be 1, 2 or 3 for a given Σ . Likewise, there exists a surface density equilibrium solution, $d\Sigma/dt = 0$, which, at a given Σ , only ever has one solution. When considering the $\Sigma - T_c$ phase-space, the thermal equilibrium curve is S-shaped while the surface density equilibrium curve is a monotonically decreasing function of Σ . For brevity we will henceforth refer to the surface density equilibrium solution as the Σ -nullcline and the thermal equilibrium curve as the T -nullcline.

The intercept of the two nullclines corresponds to a true fixed point of the dynamical system. The disk is capable of processing the mass it receives in a steady manner, and energy is produced and leaves the system at the same rate. If the intersection occurs on the upper (or lower) branch of the S-curve then the equilibrium is stable and the system remains there indefinitely. If the intersection occurs on the middle branch then the equilibrium is unstable, and if slightly perturbed the system falls into a pattern of periodic orbits (limit cycles). Such systems are identified with the classical U Gem class of variables. There are two bifurcation points, located at the two corners of the S-curve (the saddle nodes). As a control parameter is varied, \dot{M} or possibly R , the intersection point may drop from the upper branch, pass through the left-most saddle point, and then fall upon the unstable middle branch. Such a transition corresponds to a ‘global Hopf bifurcation’, and the system moves from a steady state to an outbursting state: the kind of dynamics we associate with a Z Cam variable. In Figure 3 we plot Σ and T nullclines for various \dot{M} , giving fixed point that are stable, marginal, and unstable.

3.1.3 Stochasticity

The model permits the inclusion of time-variability in either or both the mass transfer rate and the turbulent viscosity. A low amplitude time-dependent mass transfer may be modelled by a square wave in \dot{M} , oscillating around \dot{M}_0 with amplitude $\delta\dot{M}_0$ and period t_I . Here δ is a dimensionless parameter. Note in this case, the derivation of Equation (13) requires the disk to be in a steady state, and so W_0 must be redefined replacing \dot{M} with \dot{M}_0 .

To account for viscous fluctuations we introduce a time-varying term to α (Lyubarskii 1997)

$$\alpha(t) = \alpha_0 [1 + \beta(t)]. \quad (21)$$

In this equation α_0 is a constant value assumed to be 0.1 while $\beta(t)$, after time discretization, is the fluctuating term given by the Markov chain

$$\beta^n = b_0 u^n, \quad (22)$$

where b_0 is a parameter that determines the noise amplitude. The subscript n gives the time-step in fluctuation times and

$$u^n = \tilde{\alpha} u^{n-1} + \epsilon^n, \quad (23)$$

where $\tilde{\alpha}$ is another parameter chosen with the requirement that $|\tilde{\alpha}| < 1$, to ensure that the Markov chain does not diverge, and ϵ^n is a random variable taken from a uniform distribution on the range (0, 1). This process has been used in

previous studies to model disk fluctuations (King et al. 2004, Janiuk & Misra 2012), but other simpler prescriptions would also have sufficed. The mean number of timesteps between oscillation peaks is given by

$$N_{\text{step}} = \frac{2\pi}{\cos^{-1}[-1(1 + \tilde{\alpha})/2]} \quad (24)$$

and the amplitude of the oscillations is such that

$$\text{Var}(u^n) = \frac{\text{Var}(\epsilon^n)}{1 - \tilde{\alpha}^2}, \quad (25)$$

see King et al. (2004) for more details. We use $\tilde{\alpha} = -0.5$ which gives $N_{\text{step}} \approx 2.6$ and $\text{Var}(u^n) = 0.25$.

For illustrative purposes, later in this section we also employ a white noise model for β , so that $\beta = b_0 dW$, where dW is a Wiener process.

3.2 Results: classical

Before we approach the stochastic case, we consider the deterministic non-fluctuating system ($\beta = 0$) to illustrate thermal limit cycles representative of U Gem variables and, if mass transfer is included, Z Cam variables. In this section we set the central mass $M = M_\odot$, the annulus width $\Delta R = 3 \times 10^9 \text{cm}$, $R = 2.8 \times 10^{10} \text{cm}$, and $R_* = 3 \times 10^9 \text{cm}$.

3.2.1 U Gem type simulations

In a U Gem system, \dot{M} must be sufficiently small such that the Σ -nullclines, i.e. steady solutions to Equation (15), intersect the T -nullcline on the middle unstable branch at some disk radius. Let us centre our annulus at such a radius. Figure 4a exhibits a phase plane with this property. Here the T and Σ nullclines are given by the green and blue curves, respectively. The purple fixed point, their intersection, is unstable and so the system admits periodic orbits.

Let us assume that the disk annulus is initially on the low branch. Mass is being fed into the annulus at a greater rate than it is able to process it and so mass accumulates and Σ increases. Eventually, the annulus reaches the low temperature bifurcation point and leaps to the high hot state. The annulus, now above the Σ -nullcline, begins losing mass because its accretion rate exceeds the supply rate. Once the high temperature bifurcation point is reached, the annulus drops to the low temperature state and the process is repeated.

The red curve in Fig. 4a corresponds to a numerical simulation of Eqs (15) and (17) and illustrates this basic behaviour quite clearly. In Figure 4b we plot the evolution of Σ and T_c as a function of time. Here one can observe the two time-scales at work, especially in the (blue) T_c curve. In between outbursts there is little change in temperature, but a build up in mass (seen in the red curve) occurring on the slow viscous timescale t_Σ . Interleaving these phases are the abrupt bursts occurring on the short thermal timescale t_{th} .

3.2.2 Z Cam type simulations

Z Cam variables intermittently behave in a similar manner to U Gem variables but occasionally remain on the high temperature branch in a quasi-steady state for months to years before dropping to quiescence and undergoing a fresh

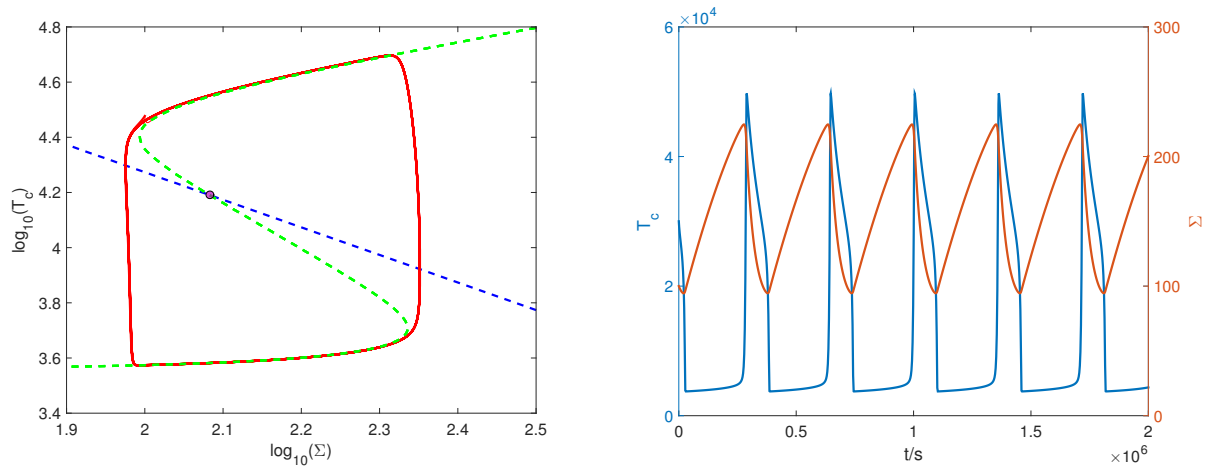


Figure 4. Both panels correspond to a ‘U Gem simulation’ with $\dot{M} = 3.8 \times 10^{16} \text{ g s}^{-1}$ and $b_0 = 0$. Left panel (a): Trajectory of a disk annuli through the $\Sigma - T_c$ phase space (red). The thermal equilibrium curve (dashed green curve) and mass nullcline (dashed blue line) are superimposed. The fixed point is shown by the purple dot. Right panel (b): Evolution of T_c and Σ as functions of time.

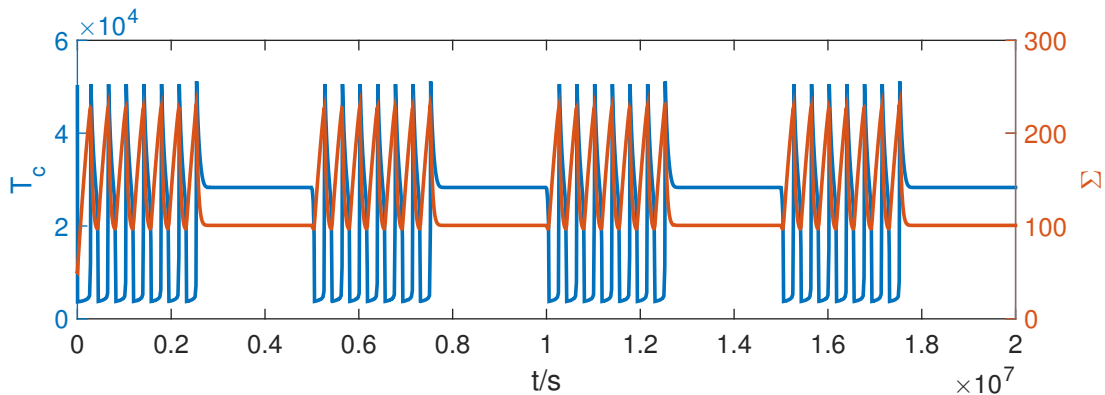


Figure 5. Time evolution of the surface density and central temperature with $\dot{M}_0 = 4 \times 10^{17} \text{ g s}^{-1}$ and $b_0 = 0$ with mass transfer variation. The variation amplitude is $\delta = 0.1$ and $t_I = 5 \times 10^6 \text{ s}$. The system clearly switches between outburst trains and standstills.

batch of outbursts. This is attributed to a shift in the Σ -nullcline upwards (due to a change in mass transfer, $\delta \neq 0$), so that the intersection is beyond the saddle node. Of course, the system must be close to criticality if this is to be possible.

To demonstrate this in our model, \dot{M}_0 and δ are chosen such that the fixed point oscillates between the stable high temperature branch and the unstable branch. When the fixed point is on the upper branch the system is stable and will remain in a standstill. A decrease in \dot{M}_0 pushes the fixed point onto the unstable branch and the system undergoes periodic orbits resulting in trains of outbursts. In Figure 5 we show an example of standstill-outburst-train cycles.

3.3 Results: stochastic

With the basics established, we include a fluctuating viscosity ($\beta \neq 0$). The fluctuation time scale is taken to be $10t_{orb}$, which is motivated by MRI shearing box simulations (Hawley et al 1995). The amplitude is set at $b_0 = 0.1$. First, we consider the case where there is no mass transfer variability ($\delta = 0$). To obtain a fixed point on the high temperature branch close to the bifurcation point we choose

$\dot{M} = 5 \times 10^{16} \text{ g s}^{-1}$. A deterministic system with this configuration would remain in the high temperature state indefinitely. A stochastic system, however, will see the fixed point jostle about as the two nullclines fluctuate with α , sometimes falling on the upper branch, sometimes dropping to the middle branch of the S-curve. The Σ -nullcline is perhaps most sensitive to viscous fluctuations because equilibria upon it obey $T_c \sim \alpha^{-1}$.

A series of 4 stochastically excited outbursts is plotted in the phase space of $\Sigma - T_c$ in Figure 6, and as a function of time in Figure 7a. The disk annulus initially hangs around the fixed point for $\approx 1.2 \times 10^6 \text{ s}$ before being stochastically excited, transitioning to the cooler branch, and undergoing limit cycles. During the dynamical phase of the cycle, there are small fluctuations around the stable manifold due to the variable α but they have little effect on the overall dynamics. It is when the system is close to the fixed point that the fluctuations become important, ultimately causing excitation of the system.

Note the slightly delayed rise to outburst at the bottom right corner of the S curve in Figure 6, near the saddle node. This is a delay brought about by the stochastic noise, and was witnessed in earlier MRI simulations (Latter & Pa-

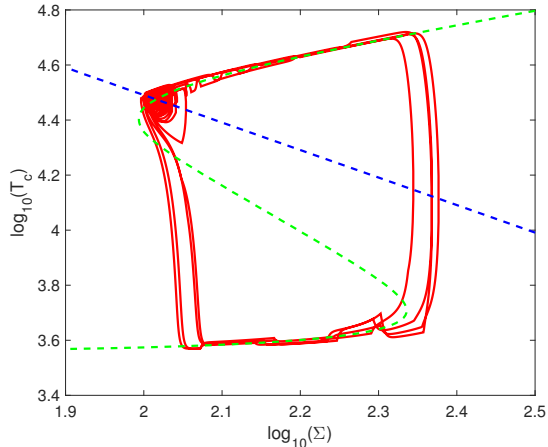


Figure 6. Time evolution (red) of a disk annuli through the $\Sigma - T_c$ phase space. For the simulation, $\dot{M} = 5 \times 10^{16} \text{ g s}^{-1}$ and $b_0 = 0.1$.

paloizou 2012, Hirose et al. 2014). The system, of course, is held up for much longer at the top left corner, because of the stable fixed point. This region is discussed in more detail in the next subsection.

3.3.1 Basins of attraction

In a deterministic dynamical system the local basin of attraction of a stable fixed point is the region in phase space defined so that if a trajectory begins in this region it will immediately return to the fixed point. In Figure 8 we plot deterministic trajectories through phase space started in the vicinity of the fixed point. The figure indicates that there is a critical curve between regions where the outburst trajectories lie and those that are attracted to the fixed point — somewhere between the two closest black and red curves. This is the leftmost boundary of the local deterministic basin of attraction. (Note that the whole phase space is within the *global* basin of attraction.)

In a noisy system, such as ours, it is possible for fluctuations to perturb a trajectory initially resting on the fixed point beyond the critical boundary, at which point it will undergo an outburst. The fluctuation must, however, be sufficiently large and/or the fixed point sufficiently close to the boundary. For fluctuations written in terms of a Markov chain, as is the case here, it is non-trivial to estimate the noise amplitude that is necessary for excitation. However, if β is assumed to be white noise instead, then the problem is more analytically tractable. In fact this has been tackled for the FHN model where ‘confidence ellipses’ can be calculated. A confidence ellipse of probability p corresponds to an ellipse in phase space enclosing the fixed point in which there is probability p of finding the solution at time t . In the Appendix we describe how these may be calculated.

In Figure 9 two close-ups of the fixed point are shown. These include (a) deterministic trajectories which help indicate the boundary of the basin of attraction (solid black and purple), (b) the two nullclines (dashed blue and green), (c) sample trajectories from a stochastic simulation (red), and finally (d) 85% confidence ellipses enclosing the fixed

points (dotted blue). The left panel corresponds to white noise of amplitude $b_0 = 0.5$ and the right panel to more vigorous noise, $b_0 = 0.9$. In the left panel the confidence ellipse is well within the basin of attraction, and indeed the red trajectory remains trapped around the fixed point. In the right panel the confidence ellipse is larger, on account of the larger amplitude noise, and straddles the basin’s boundary. As a result, trajectories can undergo outbursts, because the fluctuations aperiodically expel them from the fixed point’s basin of attraction. Indeed, we see here the red trajectory leave the vicinity of the fixed point and disappear out of the figure.

3.3.2 Parameter dependence

In this one zone model there are various parameters that may affect the evolution of the disk annulus. Here we focus on b_0 , \dot{M} and the fluctuation timescale, t_f .

In the four panels of Figures 7 we show the effect of changing b_0 and \dot{M} . The value of \dot{M} , along with the radial location, determines the intersection of the two nullclines, which in turn gives the fixed point. There exists a critical mass transfer rate \dot{M}_{crit} (for this set-up $\approx 4 \times 10^{16} \text{ g s}^{-1}$) above which the fixed point is stable and below unstable. Obviously we are interested in $\dot{M} > \dot{M}_{crit}$. Increasing \dot{M} results in the fixed point moving to higher T_c and Σ and hence moving it away from the bifurcation point. In Figure 7 we see that this has the effect of decreasing the outburst frequency by increasing the basin of attraction: the top left panel exhibits fewer outbursts than the top right panel. The amplitude of the fluctuations is given by b_0 , increasing this improves the chance of excitation, as evident in the bottom panels of Fig. 7. For sufficiently small b_0 no cycles occur because the fluctuations are insufficiently intense to perturb the system into the outburst region. It is clear that a wide range of outburst-limit cycles variation can be achieved - from U Gem (Figure 7b) to outburst/dip pairs (panel d). Note that sufficient noise amplitude permits U Gem type behaviour for mass accretion rates somewhat above the critical value derived from the classical theory.

In Figure 10a we investigate how the number of outbursts, N , in a given duration of time depends on b_0 and \dot{M} . For $\dot{M} < \dot{M}_{crit}$ the system performs cycles even in the deterministic case. In this region, increasing b_0 marginally increases N . For larger \dot{M} , the deterministic system is stable but there exists a critical b_0 above which the system is stochastically excitable. This threshold is an increasing function of \dot{M} . The reason for this is that as \dot{M} increases, a larger ‘kick’ is necessary to perturb the system sufficiently out of the local basin of attraction for the fixed point. If b_0 is increased further, N begins to plateau as a result of the finite limit cycle period. The range in b_0 , over which N increases, for a given \dot{M} , increases with \dot{M} .

In all of the above we have kept the fluctuation timescale, t_f , fixed at $10t_{orb}$. This choice is motivated by numerical simulations of MRI turbulence but is not terribly well constrained and is dependent on the physics included. In fact, fluctuations should occur over a range of timescales. In Figure 10b we explore the effect of changing this timescale, fixing $\dot{M} = 5 \times 10^{16} \text{ g s}^{-1}$ but varying b_0 . In a similar way to Figure 10a, we explore the b_0 - \dot{M} parameter space by counting the number of outbursts in a given time interval. For

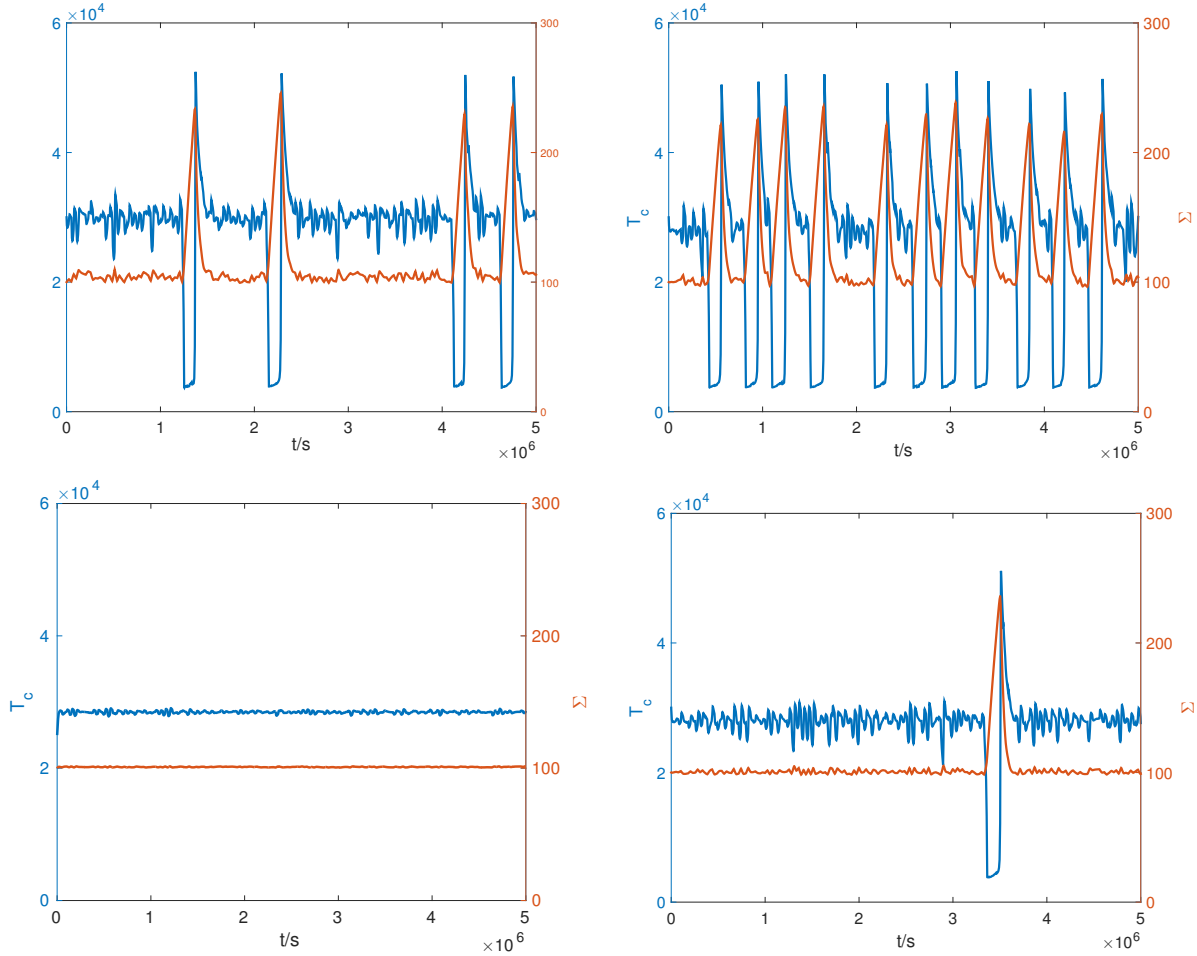


Figure 7. Evolution of central temperature T_c (blue) and surface density Σ (red) as functions of time. Top left panel (a) has $\dot{M} = 5 \times 10^{16} \text{ g s}^{-1}$ and top right panel (b) $\dot{M} = 4.55 \times 10^{16} \text{ g s}^{-1}$, both with $b_0 = 0.1$. Bottom panels have $\dot{M} = 4.55 \times 10^{16} \text{ g s}^{-1}$ with (c) $b_0 = 0.01$ (left) and (d) $b_0 = 0.05$ (right).

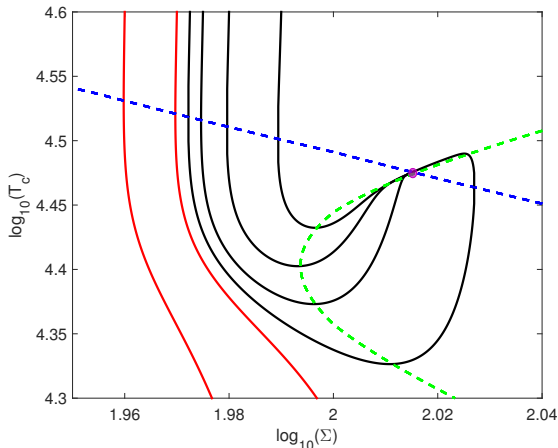


Figure 8. Right Panel: Deterministic trajectories close to the fixed point. Trajectories that undergo a full cycle are shown by the red lines and those that are immediately attracted to the fixed point are shown by the black. The fixed point is shown by the purple dot.

$t_f < 2t_{orb}$ there are no outbursts for the range of b_0 considered, this is because the system has insufficient time to adjust to the variation in α , given that the characteristic timescale for Σ is $t_\Sigma \approx 20t_{orb}$. For larger t_f the system has longer to adjust to the fluctuations but also the probability of getting a large cumulative fluctuation in a given time interval decreases. The timescale for which the number of counts is maximum is determined by the competition between these two trends. For $b_0 > 0.1$, the number of counts peaks at approximately $t_f = 8t_{orb}$ before decreasing with t_f . Unsurprisingly, the peak is at less than t_Σ given that variations in α have an amplitude much less than α_0 .

3.3.3 Mass transfer variability

Slowly varying the mass transfer rate from the secondary translates the Σ -nullcline vertically and with it the position of the fixed point. Consider the deterministic situation. If at some instance during a mass transfer cycle, the fixed point lies on the unstable manifold then outbursts can occur (Figure 5), if not, then the system will remain in either the high or low state. Fluctuations will have limited impact on the first situation other than marginally altering the outburst

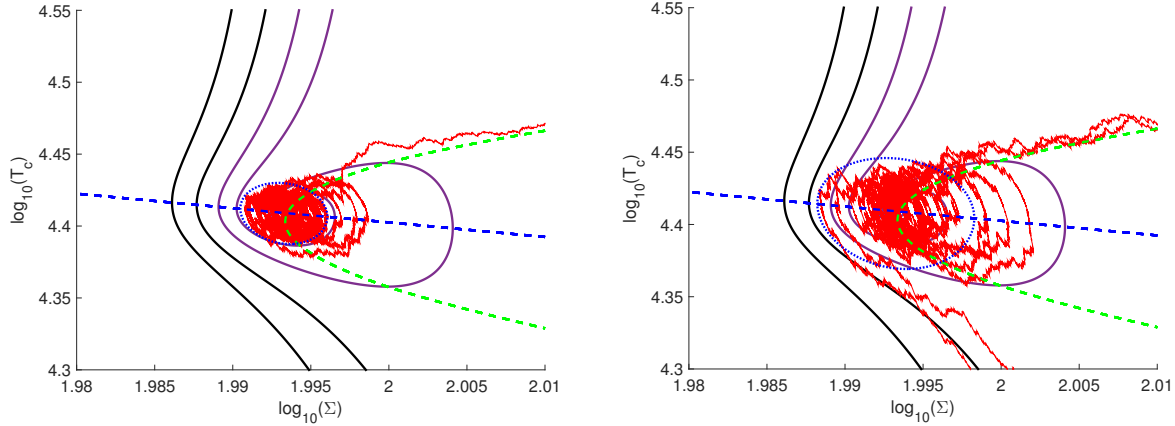


Figure 9. Here $\beta(t)$ is a Wiener process with $b_0 = 0.5$ and 0.9 , and $\dot{M} = 4 \times 10^{16} \text{ g s}^{-1}$. Confidence ellipses of 85% are shown in dotted blue along with the nullclines in dashed green and blue. Deterministic trajectories are shown by the black and purple lines, black indicates a trajectory performing a limit cycle and purple indicates a solution attracted directly to the fixed point. Finally, the red curve is the simulated trajectory.

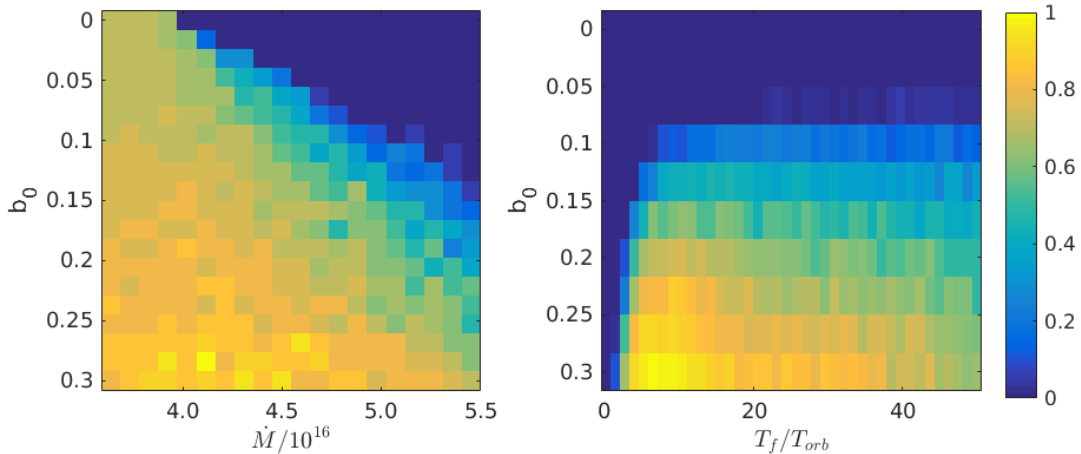


Figure 10. Both panels show the number of outbursts normalised by the maximum number of outbursts that occur during an interval of $5 \times 10^7 \text{ s}$ over the whole phase space shown using the one-zone model. Left panel (a): fluctuation amplitude and the mass accretion rate are both varied while t_f/t_{orb} is fixed at 10. Right panel (b): fluctuation amplitude and timescale are varied while the mass accretion rate is kept fixed, $\dot{M} = 5 \times 10^{16}$.

duration and magnitude. In the second case, the fluctuations can cause excitations and the dynamics are thus altered.

The parameters in Figure 11 are chosen such that the deterministic model flips between a stable state and one only just below the saddle node, and hence unstable. (However, we have achieved similar behaviour with the range of \dot{M} fully confined to the stable branch.) Here $\dot{M}_0 = 4.5 \times 10^{16} \text{ g s}^{-1}$, and we introduce a small periodic mass transfer variation with $\delta = 0.1$ and $t_f = 5 \times 10^6 \text{ s} \approx 60$ days. As with the classical model, a small and easily achievable variation in mass transfer (Viallet and Hameury, 2008) is sufficient to produce clear transitions between standstills and outburst trains when viscous fluctuations are included. The inclusion of fluctuations has three effects: it breaks the periodicity of the lightcurves, allowing variation in the number of limit cycles in each outburst train; the range of possible \dot{M} that

can undergo limit cycles is somewhat extended; and during standstills the system undergoes isolated outburst/dip pairs. The modelled behaviour does indeed do a reasonable job at reproducing most of the features of Z Cam outbursts.

3.4 Summary

Clearly the one-zone model is a vast simplification of a real astrophysical disk. One drawback is its inability to capture interactions between adjacent annuli. In addition, even though we make a wide parameter sweep, the noise amplitude and timescale are input parameters. To make further progress these inputs must be constrained. That being said, the one zone model provides a qualitatively clear representation of a disk annulus in the outer regions of a steady

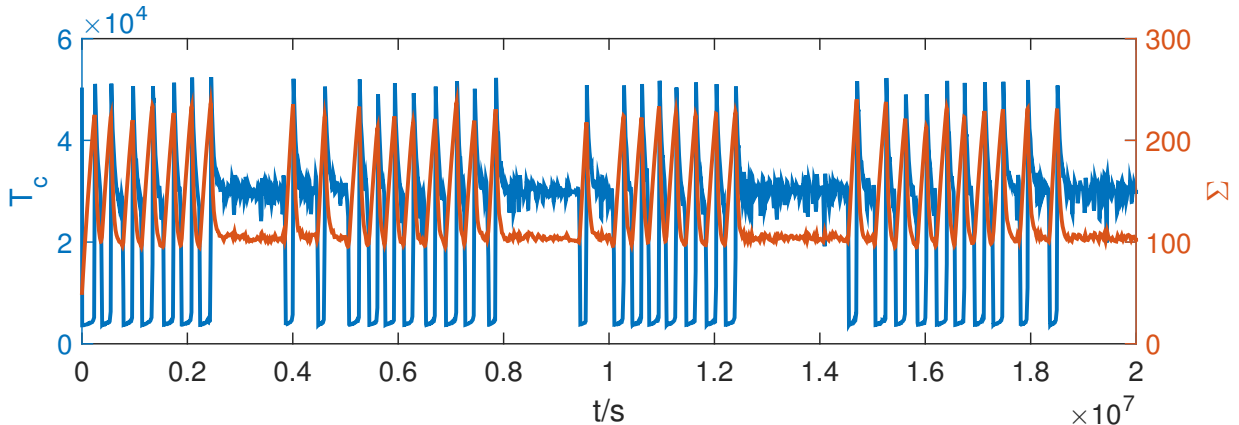


Figure 11. Simulation including mass transfer variation, $\dot{M} = 4.5 \times 10^{16} \text{g s}^{-1}$ with $\delta = 0.1$, $T = 5 \times 10^6 \text{s}$ and $b_0 = 0.1$.

state disk and hence provides a simple means of studying the effect of viscous fluctuations on instability.

Allowing for the model’s drawbacks, it is clear that introducing stochastic fluctuations alters the properties of the dynamical system. In particular, stochastic variations in α can cause the excitation of a deterministically stable system that is at a fixed point lying sufficiently close to the global bifurcation point. This results in the system following a periodic orbit before returning to its fixed point. Once an annulus has been excited the flux through it will change, adjacent annuli must then respond and may themselves undergo transitions leading to the propagation of transition waves through the disk.

4 VISCOUS GLOBAL MODEL

The previous section shows that an isolated disk annulus is excitable by stochastic variation in α . Obviously the local model is an idealisation: while in a steady state the approximation is somewhat justified, but as soon as the mass supply rate is altered on a short timescale compared to the viscous timescale, or there exists steep temperature gradients such as during the propagation of a transition wave, it breaks down. Additionally, radial energy flux to and from adjacent annuli may stabilise a local thermal runaway before a transition wave can be triggered. It is therefore necessary to check that the outburst variability is not limited to local models but can in fact result in global-disk limit cycles. In this section we take the next natural step by extending this idea into a global-disk setting. We evolve the vertically integrated time dependent 1D thin disk equations (2) and (3) along with the supplementary equations (4) - (11) and (12).

4.1 Viscosity

Again we adopt the α formalism for the viscosity but also allow for its spatial variation. It is well known that a multi-valued α is needed to explain the observed outburst durations and luminosity magnitude changes in DNe (Smak 1984). We use $\alpha_0 = \alpha_L = 0.01$ for the low temperature state and $\alpha_0 = \alpha_H = 0.1$ for the high temperature state. α has a stochastic component, β , which is a function of radius

as well as time. Therefore, Equation (21) becomes

$$\alpha(t, r) = \alpha_0(t, r) [1 + \beta(t, r)] \quad (26)$$

where

$$\alpha_0(t, r) = \begin{cases} \alpha_L, & \text{if } T_c(t, r) \leq 10^4 \\ \alpha_H, & \text{if } T_c(t, r) > 10^4. \end{cases} \quad (27)$$

We assume that compressibility plays a central role in determining the lengthscale of radial coherence in the effective viscosity and take this scale to be the pressure scale height, $H(t, r)$ (Shakura & Sunyaev, 1973). The timescale over which the fluctuations occur is set to be a function of radius given by $t_f(r) = Ct_{orb}(r)$ where C is a constant.

In order to prevent abrupt discontinuities, we apply a slight spatial and temporal smoothing to the stochastic term. Upon discretization,

$$\beta_i^n = b_0(1 - c_i)(0.6u_i^n + 0.2u_{i-1}^n + 0.2u_{i+1}^n) + c_i\beta_i^k \quad (28)$$

where u_i^n is the Markov process, given by Equation (23), at radial grid element i at timestep n , and k is the most recent timestep at which u_i was updated. Note that u_i^n is constant over radial intervals of order H and is updated every t_f . The c_i ’s are functions of time chosen such that a linear smoothing occurs over $t_f/10$. Physically, it is likely that there are neither instantaneous changes nor abrupt discontinuities in the radial direction given the properties of the large-scale MRI dynamo. Large-scale interactions (Guan et al 2009), magnetic field linkages and compressive waves may also mediate spatial variations.

4.2 Numerics, mass input, and boundary conditions

We evolve Equations (2) and (3) using a finite difference scheme on a fixed logarithmically spaced grid of 200 points. The advective term is solved using an upwind method and we use multi-time-stepping for the radial radiative energy transport term. The timestep is constrained by the most stringent condition: the diffusive and advective CFL conditions and a constraint coming from the local heating and cooling terms. The outer disk edge is set at $3 \times 10^{10} \text{cm}$ and the inner edge at $3 \times 10^9 \text{cm}$. The boundary conditions are chosen for simplicity: for the surface density we adopt

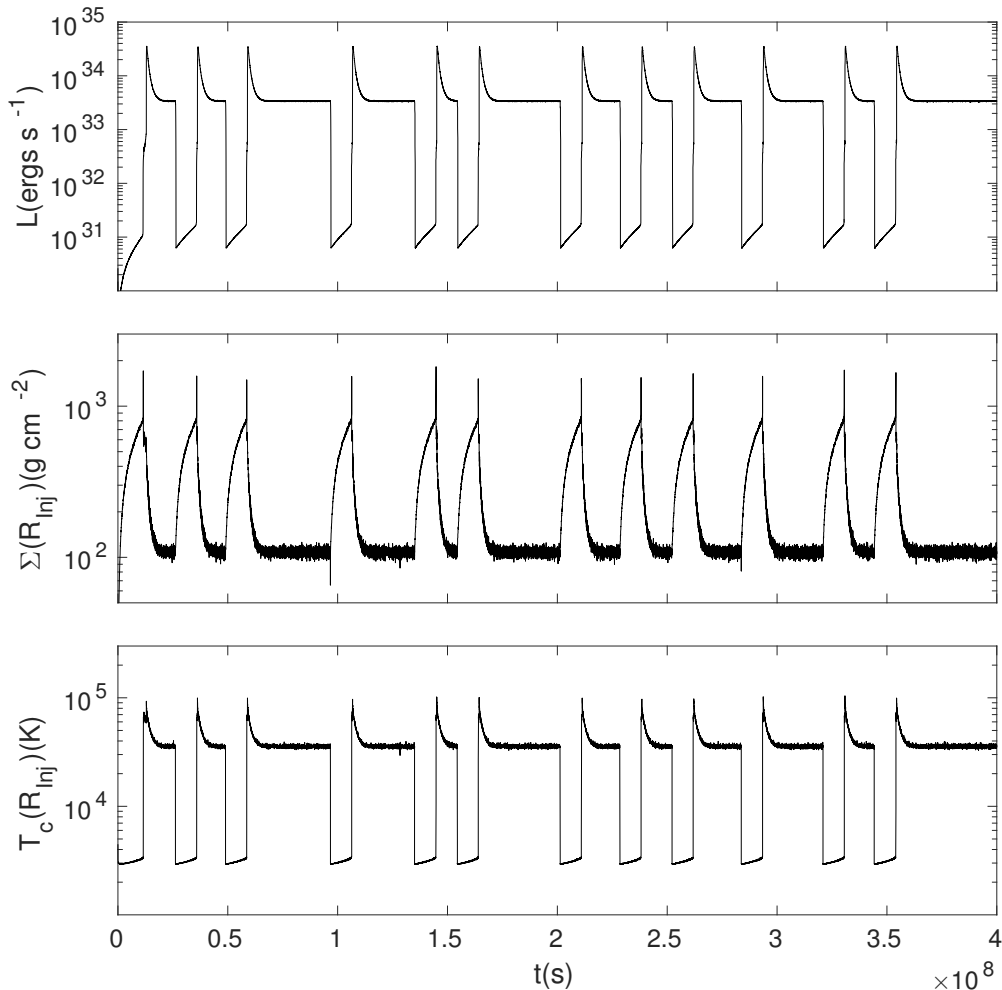


Figure 12. Lightcurve from simulations with a mass injection rate of $1.1 \times 10^{17} \text{ g s}^{-1}$, $b_0 = 0.125$ and $t_f = 10$. Note the variable length of the standstills after each outburst, which differs from the (comparably regular) viscous timescale of quiescence.

$\Sigma(r_{in}) = 0$ for the inner boundary, and the analytic solution to the thin-disc equations for the outer boundary. The thermal energy equation is second-order in r and so two boundary conditions are necessary. However, as pointed out by Hameury et al. (1998), higher order terms are of minimal importance other than at transition fronts, and it is the local heating and cooling that dictate what is going on. The boundary condition hence has minimal effect and we take $\partial T_c / \partial r = 0$. Via the term S , we inject mass uniformly at a rate \dot{M} in the range $2.4 \times 10^{10} \text{ cm} < r < 2.5 \times 10^{10} \text{ cm}$.

Turbulent fluctuations have a coherence length set to the scale height, H , as described earlier. When H decreases below the grid size, we account for averaging over a larger change in radius by introducing a factor $H/\Delta R$ where ΔR is the radial bin size. We also introduce a buffer zone between $r < 6 \times 10^9 \text{ cm}$ and $r > 2.8 \times 10^{10} \text{ cm}$ to safeguard against stochastic effects at the boundary. Finally, we commence our simulations with a small initial surface density, $\Sigma = 1 \text{ g cm}^{-2}$, and a temperature of 3000 K .

4.3 Luminosity

Light curves are calculated using the bolometric luminosity defined through

$$L = 2 \int_{r_{in}}^{r_{out}} 2\pi F_s r dr, \quad (29)$$

allowing for comparison with observations. Note that the luminosity is dominated by contributions from the inner regions due to the functional form of the emitted flux, and the radially decreasing temperature profile.

4.4 Results

Given that the outer regions are more susceptible to downward transition we choose parameters such that the whole disk is in the hot state but the annuli near the outer edge are close to criticality – only marginally hotter than the upper bifurcation point. For our configuration this corresponds to $\dot{M} \sim 1.1 \times 10^{17} \text{ g s}^{-1}$. While the system is on the hot branch, the state that we are primarily interested in,

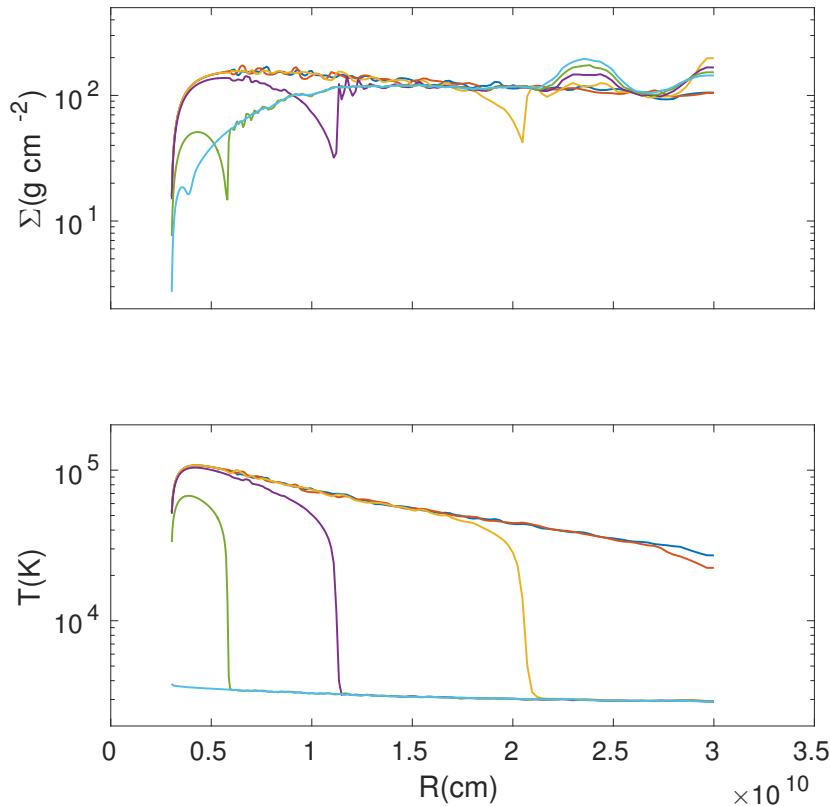


Figure 13. Radial Σ and T_c profiles for the same simulation as in Figure 12 during the excitation of a cooling wave. The profiles are separated by 10^9 s starting with the dark blue curve, proceeding through red, yellow, purple, green and ending with light blue.

$H \sim 2\Delta R$ except at the inner boundary. During quiescence, typically $H \sim 0.5\Delta R$.

For our first simulation we use $t_f/t_{orb} = 10$, $b_0 = 0.1$, a choice that is motivated by our parameter study in Section 3. The resulting lightcurve is plotted in the top panel of Figure 12. For the majority of the simulation, the disk is in a high luminosity state but occasionally transitions to a quiescent state two orders of magnitude less luminous. The durations of quasi-steady periods range from $\lesssim 1 \times 10^7$ s to $\gtrsim 4 \times 10^7$ s, while the quiescent phase lasts for $\lesssim 1 \times 10^7$ s.

In the middle and lower panels of Figure 12 we show the time evolution of Σ and T_c at the outermost injection radius, $r = 2.5 \times 10^{10}$ cm. Qualitatively the behaviour at this radius is similar to that in the one-zone model. The most noticeable difference is the spike in the density that precedes the transition to the hot state which is a result of the passage of the pre-transition density wave (Papaloizou et al. 1983). The timescale amplitude is due to the different imposed α in the low state.

Upon closer inspection, we find, as expected, that the cooling wave originates close to the outer boundary where the disk is more susceptible to downward transition, Figure 13. This feature is due to the shift of the local T -nullcline towards higher surface densities and the concurrent movement of the local Σ -nullcline to lower surface densities. Once triggered by a downward transition, a cooling wave, along with its preceding density rarefaction wave (Papaloizou et al

1983), travels inward and propagates through the full radial extent leaving the whole disk in the low temperature/weakly accreting state with a much depleted surface density at small radii. As this wave has an interface of length $\sim H$ one may expect appreciable pressure gradients and consequent wave launching, which may be significant in the dynamics, though not captured by the 1D diffusion model.

The minimal variation during the quasi-steady phases shown in the lightcurve is a direct result of our inner buffer-zone. More precisely, the emitted flux, $\propto T_e^4$, is a steep function of r for $r \gtrsim 4 \times 10^9$ cm with its maximum inside our buffer region.

The propagation distance of the cooling wave through the disk is dependent on α_H and α_L (Smak 1984). Reduction of this ratio from $\alpha_H/\alpha_L = 10$ decreases the propagation distance of the cooling wave through the disk and leads to reflection of the cooling wave at some radius. This shortens and reduces the amplitude of the luminosity drop, leading to sawtooth shaped lightcurves (Papaloizou et al 1983).

4.4.1 Fluctuation amplitude

To observe the effect of the fluctuation amplitude on excitability, we fix $\dot{M} = 1.1 \times 10^{17}$ g s $^{-1}$ and $t_f = 10t_{orb}$ but change b_0 . Light curves from simulations with various b_0 between 0.075 and 0.15 are shown in Figure 14. As with the one-zone model, the sensitivity to b_0 is apparent. For

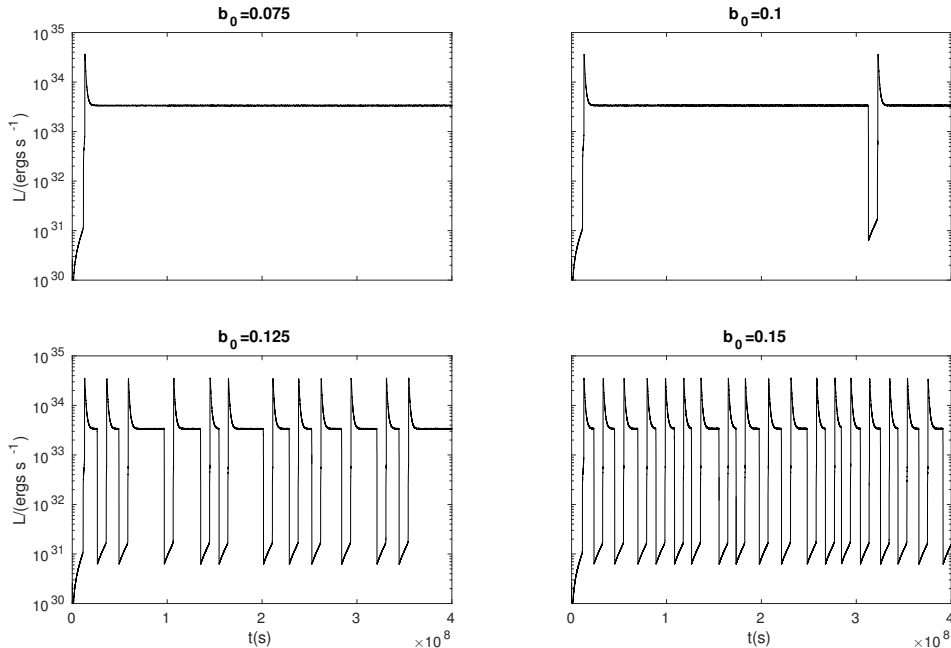


Figure 14. Lightcurves from 1D simulations with $\dot{M} = 1.1 \times 10^{17} \text{ g s}^{-1}$ and $t_f/t_{orb} = 10$.

this configuration, $b_0 < 0.1$ is unable to excite the system. However, for $b_0 \gtrsim 0.15$ the disk undergoes near continuous limit cycles more reminiscent of a U Gem system, but with some variability in outburst length and occurrence. This shows again that stochasticity can transform a ‘stable’ system into a U Gem system if the noise amplitude is sufficiently large. For a somewhat limited intermediate band in b_0 , the steady state durations are highly non-uniform ranging between $3 \times 10^6 \text{ s}$ and $5 \times 10^7 \text{ s}$. We hence do not reproduce classical Z Cam behaviour: both the standstills and outburst trains are of too short a duration in comparison with observations.

4.4.2 Fluctuation timescale

In the one-zone model, fluctuations on timescales of $\lesssim t_\Sigma$ lead to the most regular outbursts. What is the timescale equivalent to t_Σ in the global disk simulations? The one zone model states that $t_\Sigma \sim (\Delta R)^2$. In a global disk the natural choice for ΔR would be the turbulent lengthscale which we take to be $\sim H$. However, in our simulations we have a buffer zone at the outer edge and it is the outer edge that goes unstable first, hence, a more apt choice is $\Delta R \sim H + \Delta R_{\text{buff}}$. The surface density of this whole annulus must evolve driven by fluctuations in density at the outermost fluctuating orbit. With this we obtain $t_\Sigma \approx 30t_{orb}$ for the diffusion timescale of interest. Therefore we expect the most regular excitations when $t_f \lesssim 30t_{orb}$. Note that this is much less than the viscous timescale if defined with respect to the whole disk.

In Figure 15 we plot lightcurves for a range of t_f/t_{orb} at fixed fluctuation amplitude and mass injection rate. It is clear that if the fluctuation timescale is too short, $t_f \ll t_\Sigma$,

then excitations are unlikely/impossible. The outer disk is unable to adapt to the fluctuations sufficiently quickly. For t_f closer to t_Σ , excitation becomes more likely. The t_f at which the disk is most excitable appears to be $< t_\Sigma$ as was also the case in the one-zone model. Increasing t_f further leads to less frequent outbursts as the disk annulus is able to adapt to the fluctuation on a shorter timescale than t_f , resulting in idle time before the next ‘kick’. Evidently long timescale fluctuations are unnecessary, and furthermore non-optimal, for causing stochastic excitation; $t_f \lesssim H^2/\nu$ suffices.

5 DISCUSSION

In this paper we study the stochastic excitation of DN accretion disks caused by fluctuations arising from disk turbulence as opposed to the more classical mass transfer variation. The systems of particular interest here are the class of Z Cam variables. We intend this work to be a proof of concept and so adopt simple local and 1D global time-dependent models. The radiative and ionisation physics is approximated by a vertically integrated cooling law (FLP), which is simple to implement and physically motivated (though omits some of the detailed physics).

First, we solve a one-zone system of stochastic differential equations for the surface density and central temperature. DNe that would otherwise remain indefinitely in a quasi-steady state can perform limit cycles when the stress is allowed to be stochastic. The duration of standstills prior to excitation depends strongly on the fluctuation amplitude and the amount that the mass injection rate exceeds the critical value determining stability. Introducing a subcritical mass transfer rate (insufficiently strong to cause transi-

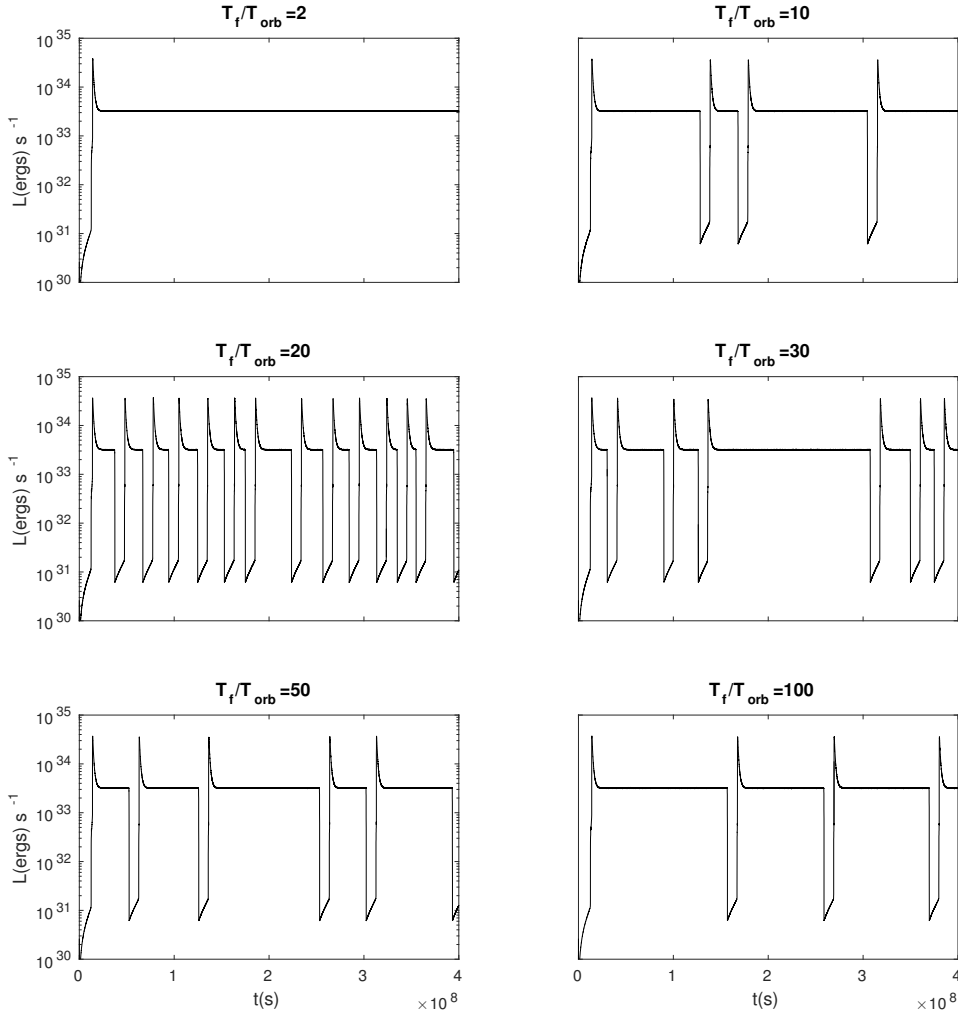


Figure 15. Lightcurves from simulations with $\dot{M} = 1.05 \times 10^{17} \text{ g s}^{-1}$ and $b_0 = 0.075$ and various t_f .

tions between cycles and steady state behaviour) together with the fluctuations lead to trains of outbursts separated by standstills. The standstills, however, are somewhat shorter than observed, or the outburst trains not especially long. It is, however, relatively easy to obtain aperiodic singular outbursts.

Our second model is a 1D viscous time-dependent model, similar (but somewhat simpler) than those currently used (e.g. Cannizzo 1993a). We find that the outer regions of a disk with a marginally supercritical mass supply rate can be stochastically excited. Between excitation, the standstills in the high state are found to last between several hundred days to a few years. The transition from high to low states first occurs at the outer boundary resulting in an inward propagating cooling wave. When the average α in the low state is taken to be much less than that of the high state the cooling wave can propagate throughout the entire disk leading to decreases in luminosity of ~ 2 mag. For more com-

parable α 's the cooling wave is reflected in the bulk of the disk.

The results presented in this paper suggest that fluctuations in accretion rate can trigger isolated drops from steady state to quiescence and then back. The behaviour is reminiscent of the singular outburst/dip pairs found in some Z Cams, and possibly the stunted outbursts in Nova like variables (Honeycutt et al 1998, Honeycutt 2001). We believe it is natural to attribute these events to disk fluctuations. The mechanism can also generate repeated outbursts amidst standstills, but either the standstills are too short (because the disk turbulence can too easily perturb the equilibrium) or the outburst trains too short to successfully match Z Cam light curves in general. Finally, sufficiently large viscous fluctuations can cause systems with stable \dot{M} to exhibit more classical U Gem type behaviour, i.e. repeated outbursts with very few to no standstills. Note that these results were obtained with only one, rather simple, noise model

and the fluctuations arising from MRI turbulence may provide a more rich set of dynamics.

We conclude that stress stochasticity on its own is not a viable replacement to mass transfer variability from the secondary in explaining essential Z Cam phenomena (Meyer & Meyer-Hofmeister 1983). This stochasticity, however, may still provide an important ingredient in their dynamics, by adding an additional level of variability in the occurrence and duration of outburst trains and standstills, and may directly excite aperiodic and isolated outburst/dip pairs. In fact, with more advanced modelling it may be possible to constrain the fluctuation amplitude via comparison with observed light curves.

ACKNOWLEDGEMENTS

The authors would like to thank the reviewer, John Cannizzo, for a set of helpful comments that improved the clarity of the paper. The work also benefited from input from John Papaloizou and Pavel Ivanov. HNL and JR are partially funded by STFC grants ST/L000636/1 and ST/K501906/1.

REFERENCES

- Bashkirtseva, I and Ryashko, L., 2011, Phys. Rev. E, 83, 061109.
 Buat-Ménard. V., Hameury. J.-M., Lasota. J. -P., 2001b, A&A, 369,925-931.
 Cannizzo, J.K., 1993a, ApJ, 419, 318.
 Cannizzo, J.K., 1993b in: Wheeler, J.C., (Ed), Accretion Disks in Compact Stellar System, World Scientific, vol. 9.
 Cowperthwaite. P. S., Reynolds. C. S., 2014, ApJ, 791:126.
 Guan, X. and Gammie, C. F. and Simon, J. B. and Johnson, B. M., 2009, ApJ, 694, 1010-1018.
 Hameury, J.M, Menou, K., Dubus, G., Lasota, J.P., Hure, J.M., 1998, MNRAS, 298, 1048.
 Hawley J. F., Gammie C. F., Balbus S. A., 1995, ApJ, 440.
 Hirose, S., Blaes, O., Krolik, J.H., Coleman, M.S., Sano, T., 2014. ApJ, 787, 1.
 Honeycutt. R., K. and Robertson. J. W., 1998, The Astronomical Journal, 116, 1961-1965.
 Honeycutt. R., 2001, PASP, 113, 473-481.
 Hōshi. R., 1979, Progress of Theoretical Physics, 61, 1307-1319.
 Ingram. A., van der Klis. M., 2013, MNRAS, 434, 1476.
 Janiuk. A., Misra. R., 2012, A&A, 540, A114.
 King, A. R., Cannizzo, J. K., 1998. ApJ, 499, 348.
 King. A. R, Pringle. J. E., West. R. G. and Livio. M., 2004, MNRAS, 348, 111-122.
 Laing, C. and Lord, G. J., *Stochastic Methods in Neuroscience*, 2010, Oxford University Press, Oxford.
 Lasota. J. P., 2001, New Astron. Rev., 45, 449.
 Latter. H. N., Papaloizou. J. C. B., 2012, MNRAS, 426, 1107-1120
 Lightman, A. P. and Eardley, D. M., 1974, ApJ, 187.
 Lin, D. N., Papaloizou, J. C. B., and Faulkner, J., 1985, MNRAS, 212, 105. (FLP)
 Linder, B. and Garcia-Ojalvo, J. and Neiman, A. and Schimansky-Geier, L., Phys. Rep., 2004 , 392, 321.
 Livio. M., Pringle. J. E., 1994, ApJ, 427, 956-960.
 Lyubarskii. Y. U., 1997, MNRAS, 292, 679-685.
 Meyer. F., Meyer-Hofmeister. E., 1981, A&A, 104, L10-L12.
 Meyer. F., Meyer-Hofmeister. E., 1983, A&A, 121, 29-34.
 Mineshige. S., Osaki. Y., 1983, Publ. Astron. Soc. Japan, 35, 377-396.

- Papaloizou. J., Faulkner. J., Lin. D. N. C., 1983, Mon. Not. R. Astr. Soc, 205, 487-513.
 Pringle. J. E., 1981, Ann. Rev. Astron. Astrophys,19, 137-162.
 Pringle, J.E., Cannizzo, J.K., 1998. Apj, 499, 348.
 Ross, J., Latter, H.N., 2017. MNRAS accepted. arXiv:1703.00211
 Shakura. N, Sunyaev. R., 1973, A&A, 24, 337-355.
 Simonsen et al., 2014, JAAVSO, 42.
 Smak. J., 1984, Acta Astron, 34, 161-189.
 Smak. J., 1996, Kluwer Academic Publishers, 45.
 Treutlein. H., Schulten. K., 1985, Ber. Bunsengens. Phys. Chem., 89, 710.
 Treutlein. H., Schulten. K., 1986, Eur. Biophys. J. 13, 355.
 Uttley. P., McHardy. I. M., 2001, MNRAS, 323, L26.
 Viallet. M., Hameury. J.-M., 2008, A&A, 489, 699-706.
 Warner, B, 1995. Cataclysmic Variable Stars, CUP, Cambridge.

APPENDIX A: CONFIDENCE ELLIPSES

The introduction of a small amount of noise renders the FN model stochastically excitable, leading to the ‘aberrant’ firing of neurons (Linder et al 2004; Laing & Lord 2010). Bashkirtseva & Ryashko (2011) were able to analytically determine noise thresholds that are necessary for excitation. Here we give a brief summary of their technique and then apply it to our local DN model.

Consider the system of stochastic differential equations

$$\dot{\mathbf{x}} = \mathbf{f}(\mathbf{x}) + b_0 \mathbf{A}(\mathbf{x}) \dot{\mathbf{w}}, \quad (\text{A1})$$

where \mathbf{x} is an n -element vector, $\mathbf{f}(\mathbf{x})$ is an n -vector function, $\mathbf{w}(t)$ is a n -dimensional Wiener process, $\mathbf{A}(\mathbf{x})$ is a $n \times n$ -matrix function, and b_0 is the disturbance intensity. If there exists an attractor when $b_0 = 0$, i.e. for the deterministic case, then a corresponding stochastic attractor with stationary probability distribution function $g(\mathbf{x}, b_0)$ exists when $b_0 \neq 0$. The *probability distribution function* $g(\mathbf{x}, b_0, t)$ is informally defined such that the probability that the solution is within $d\mathbf{x}$ at time t is given by $g(\mathbf{x}, b_0, t)d\mathbf{x}$. A *stationary probability distribution* is then a probability distribution function that is time independent, $g(\mathbf{x}, b_0, t) = g(\mathbf{x}, b_0)$.

This distribution is given by the Kolmogorov-Fokker-Planck equation which is difficult to solve in general. However, for small b_0 the distribution can be approximated by

$$g(\mathbf{x}, b_0) \approx K \exp\left(-\frac{\Phi(\mathbf{x})}{b_0^2}\right). \quad (\text{A2})$$

In the above expression $\Phi(\mathbf{x})$ is an appropriate quasi-potential and K a constant. If we assume that there is an exponentially stable equilibrium, $\bar{\mathbf{x}}$, then a quadratic approximation for the quasi-potential can be used $\Phi(\mathbf{x}) \approx \frac{1}{2}(\mathbf{x} - \bar{\mathbf{x}})^T \mathbf{W}^{-1}(\mathbf{x} - \bar{\mathbf{x}})$, where \mathbf{W} , known as the stochastic sensitivity matrix, is a positive definite matrix that is uniquely determined by

$$\mathbf{F}\mathbf{W} + \mathbf{W}\mathbf{F}^T = -\mathbf{S}, \quad \mathbf{F} = \frac{\partial \mathbf{f}}{\partial \mathbf{x}}(\bar{\mathbf{x}}), \quad (\text{A3})$$

$$\mathbf{S} = \mathbf{G}\mathbf{G}^T, \quad \mathbf{G} = \mathbf{A}(\bar{\mathbf{x}}). \quad (\text{A4})$$

From this, a confidence ellipse surrounding the fixed point can be computed from the following set of equations

$$(\mathbf{x} - \bar{\mathbf{x}})^T \mathbf{W}^{-1}(\mathbf{x} - \bar{\mathbf{x}}) = 2k^2 b_0^2, \quad (\text{A5})$$

where $k = -\ln(1 - p)$ and p is the desired probability. A *confidence ellipse* of probability p is defined as an ellipse

around the fixed point for which there is a probability p of the solution being within it at time t .

With this information it is possible to estimate the amplitude of the noise that is necessary to stochastically excite a system. Note that this treatment is only possible when the fluctuations can be modelled as a white noise, that is, the noise has a correlation time that is negligible compared to the other timescales of the system.

In order to visualize the importance of the the perturbation amplitude we calculate 85% confidence ellipses and plot them in Figure 9. The left-hand figure shows that if the confidence ellipse is contained within the local basin of the fixed point then outbursts are very unlikely if not impossible. However, if the noise amplitude is sufficiently large such that the confidence ellipse extends past the critical curve separating the local basin of attraction from the limit cycle phase space then stochastic excitation occurs. Essentially, the question of whether stochastic excitability is possible or not is determined by how likely it is for fluctuations to push the system over the critical curve and out of the local basin of attraction.